

AD-A137 378

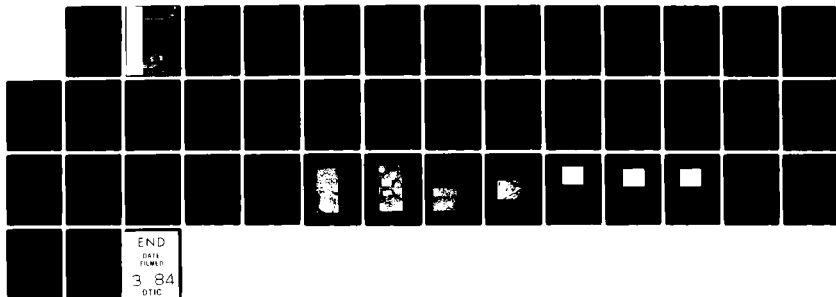
QUASI-CLEAVAGE AND MARTENSITE HABIT PLANE(U) LEHIGH
UNIV BETHLEHEM PA INST OF FRACTURE AND SOLID MECHANICS
M GAO ET AL. SEP 83 IFSM-83-122 N00014-75-C-0543

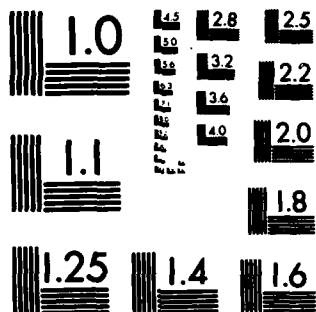
1/1

UNCLASSIFIED

F/G 11/6

NL





MICROCOPY RESOLUTION TEST CHART
NATIONAL BUREAU OF STANDARDS-1963-A

1970-11-22

UNIVERSITY



CHINESE, JAPANESE AND MANCHURIAN DRAFT PLANS

AD A 137378

King Geo and R. P. Wei

DTIC

1970-11-22

QUASI-CLEAVAGE AND MARTENSITE HABIT PLANE

by

Ming Gao¹ and R. P. Wei²
Lehigh University
Bethlehem, PA 18015

Accession For	
NTIS GRA&I	<input checked="" type="checkbox"/>
DTIC TAB	<input type="checkbox"/>
Unannounced	<input type="checkbox"/>
Justification	
By	
Distribution/	
Availability Codes	
Dist	Avail and/or Special
A-1	

Technical Report No. 16

OFFICE OF NAVAL RESEARCH



This document has been approved for public release and sale; its distribution is unlimited.

¹ Visiting Scholar, Department of Metallurgy and Materials Engineering; on leave from the Department of Materials Sciences, Shanghai Jiao Tong University, Shanghai, People's Republic of China.

² Professor of Mechanics, Department of Mechanical Engineering and Mechanics.

Unclassified

SECURITY CLASSIFICATION OF THIS PAGE (When Data Entered)

REPORT DOCUMENTATION PAGE		READ INSTRUCTIONS BEFORE COMPLETING FORM
1. REPORT NUMBER IFSM-83-122	2. GOVT ACCESSION NO.	3. RECIPIENT'S CATALOG NUMBER
4. TITLE (and Subtitle) QUASI-CLEAVAGE AND MARTENSITE HABIT PLANE		5. TYPE OF REPORT & PERIOD COVERED Technical Report No. 16
		6. PERFORMING ORG. REPORT NUMBER
7. AUTHOR(s) Ming Gao and R. P. Wei		8. CONTRACT OR GRANT NUMBER(s) Contract N00014-75-C-0543
9. PERFORMING ORGANIZATION NAME AND ADDRESS Lehigh University Bethlehem, PA 18015		10. PROGRAM ELEMENT, PROJECT, TASK AREA & WORK UNIT NUMBERS NR 036-997
11. CONTROLLING OFFICE NAME AND ADDRESS Office of Naval Research Department of the Navy Arlington, VA		12. REPORT DATE September, 1983
		13. NUMBER OF PAGES 39
14. MONITORING AGENCY NAME & ADDRESS (if different from Controlling Office)		15. SECURITY CLASS. (of this report) Unclassified
		15a. DECLASSIFICATION/DOWNGRADING SCHEDULE
16. DISTRIBUTION STATEMENT (of this Report) This document has been approved for public release and sale; its distribution is unlimited.		
17. DISTRIBUTION STATEMENT (of the abstract entered in Block 20, if different from Report)		
18. SUPPLEMENTARY NOTES		
19. KEY WORDS (Continue on reverse side if necessary and identify by block number) Fracture mechanics, fractography, steels, hydrogen embrittlement, microstructure, crystallography.		
20. ABSTRACT (Continue on reverse side if necessary and identify by block number) Quasi-cleavage (QC) is often observed on the fracture surfaces of hydrogen embrittled iron and steels. For quenched-and-tempered martensitic high strength steels, most QC facets show geometrical markings that are made up of fine oblong elements arrayed at well defined angles. To better understand this mode of failure, scanning and transmission electron microscopy (SEM and TEM) and etch-pit analysis have been applied to the study of		

DD FORM 1 JAN 73 1473

EDITION OF 1 NOV 65 IS OBSOLETE
S/N 0102-014-6001

Unclassified

SECURITY CLASSIFICATION OF THIS PAGE (When Data Entered)

Unclassified

SECURITY CLASSIFICATION OF THIS PAGE(When Data Entered)

quasi-cleavage and of martensitic structure in an AISI 4340 steel (tempered at 478 K). A special technique was developed for determining martensite habit planes without the need for concomitant presence of retained austenite or annealing twins in the microstructure.

Quasi-cleavage in this AISI 4340 steel has been shown to be cleavage along $\{110\}_\alpha$ planes through martensites, and $\{225\}_\gamma$ have been unambiguously determined as the martensite habit planes. The methods of analyses are described. The relationship between surface features of QC facets and the martensitic microstructure and the possible interaction between hydrogen and slip are discussed. Potential application of the analysis method to studies of martensitic transformation is considered.

Unclassified

SECURITY CLASSIFICATION OF THIS PAGE(When Data Entered)

QUASI-CLEAVAGE AND MARTENSITE HABIT PLANE

Ming Gao¹ and R. P. Wei²
Lehigh University
Bethlehem, PA 18015

ABSTRACT

Quasi-cleavage (QC) is often observed on the fracture surfaces of hydrogen embrittled iron and steels. For quenched-and-tempered martensitic high strength steels, most QC facets show geometrical markings that are made up of fine oblong elements arrayed at well defined angles. To better understand this mode of failure, scanning and transmission electron microscopy (SEM and TEM) and etch-pit analysis have been applied to the study of quasi-cleavage and of martensitic structure in an AISI 4340 steel (tempered at 478 K). A special technique was developed for determining martensite habit planes without the need for concomitant presence of retained austenite or annealing twins in the microstructure.

Quasi-cleavage in this AISI 4340 steel has been shown to be cleavage along $\{110\}_\alpha$ planes through martensites, and $\{225\}_\gamma$ have been unambiguously determined as the martensite habit planes. The methods of analyses are described. The relationship between surface features of QC facets and the martensitic microstructure and the possible interaction between hydrogen and slip are discussed. Potential application of the analysis method to studies of martensitic transformation is considered.

¹ Visiting scholar, Department of Metallurgy and Materials Engineering; on leave from the Department of Materials Sciences, Shanghai Jiao Tong University, Shanghai, Peoples Republic of China.

² Professor of Mechanics, Department of Mechanical Engineering and Mechanics.

QUASI-CLEAVAGE AND MARTENSITE HABIT PLANE

Ming Gao and R. P. Wei
Lehigh University
Bethlehem, PA 18015

1.0 INTRODUCTION

It is known that quasi-cleavage (QC) is one component of hydrogen assisted cracking in steels. There are increasing amounts of evidence to show that quasi-cleavage produced by internal hydrogen embrittlement in iron single crystal and steels is crystallographic and occurs on planes approximately parallel to $\{110\}_\alpha$, or $\{112\}_\alpha$, in martensite [1-8]. It has been reported also, however, that QC in steels occurred along martensite lath packets [9-13]; notably the recent reports by Costa et al. [10,11]. These investigators observed that the features of QC facets in a medium carbon steel are very much like the features of its martensite microstructure. Since the identification of cracking path is essential to the understanding of mechanisms for hydrogen assisted crack growth, a further study of QC is needed to determine if it is truly cleavage, vis-à-vis cracking along martensite lath boundaries.

In the present investigation, QC facets, produced from earlier studies of sustained-load crack growth in an AISI 4340 steel in hydrogen and hydrogen sulfide [14-16], were examined. Special emphasis was placed on the relationship between these facets and the martensite microstructure. Identification of the crystallographic orientation of QC facets was made by using an etch-pit method. The relationship between the configuration of

fine features observed on the QC facets and martensite habit planes was also determined. For this determination, a method for determining the martensite habit plane in steels, in the absence of retained austenite, had to be developed. This method is based on the combined use of crystallographic theory of martensitic transformation and of trace analyses of transmission electron micrographs of martensites.

The experimental procedures and the results of fractographic and etch-pit analyses are given first. The method for determining the martensite habit planes and its application to AISI 4340 steel are then described. The relationship between quasi-cleavage fracture facets and the martensite microstructure is then considered. Details of the crystallographic analysis procedures are given in the appendices.

2.0 EXPERIMENTAL PROCEDURES

The AISI 4340 steel used in this study is the same one used in the earlier studies on crack growth kinetics [14-16], and has extra low residual impurity content. It was laboratory vacuum melted and vacuum cast as a 100 mm thick by 305 mm wide by 560 mm long slab ingot, and was hot rolled straight-a-way to 9 mm thick plates. The chemical composition, heat treatment and room temperature tensile properties of this steel are given in Table 1. Specimen configuration and experimental procedures for determining the crack growth kinetics in hydrogen and hydrogen sulfide are given in [14-16].

Fracture surfaces produced in the crack growth studies [14-16] were examined with a scanning electron microscope (SEM) operated in the secondary electron imaging mode at 20 kV. An etch-pit method [17] was used to determine the crystallographic orientation of the quasi-cleavage facets. Etching was carried out at 298 K in an aqueous solution, containing 15 ml H_2O_2 , 2 ml HCl and 100 ml H_2O . Pits of acceptable quality were obtained after etching for 5 to 10 seconds.

To provide further identification and correlations of the fracture path with the underlying microstructure and martensite habit planes, transmission electron microscopy (TEM) was used. Thin foils were prepared by chemical thinning with a solution of 160 ml H_2O , 30 ml H_2O_2 and 10 ml HF at first. Final thinning was done by twin-jet electropolishing at 273 K and 38-40 volts (d.c.), in an electrolyte containing 515 ml of glacial acetic acid, 100 grams of sodium chromate and 50 grams of chromic acid [18].

3.0 FRACTOGRAPHIC OBSERVATIONS AND ORIENTATION OF QC FACETS

3.1 Quasi-Cleavage Features

The quasi-cleavage facets, produced by sustained-load (Stage II) crack growth in hydrogen and in hydrogen sulfide [14-16], exhibited distinct geometrical markings. A typical SEM micrograph of a QC facet is shown in Fig. 1(a), and shows the presence of such markings at a high magnification. A SEM micrograph of a polished-and-etched surface of this AISI 4340 steel is shown in Fig. 1(b) for comparison. It can be seen clearly from these two micrographs that (i) the geometrical markings are made up of fine oblong elements that are either parallel or intersect at well

defined angles, and (ii) the configuration of these elements on the QC facets resembles the microstructure of quenched and tempered AISI 4340 steel (specifically, that of martensite). This resemblance between the surface features of QC facets and the microstructure of martensitic steel was also found by Costa and Thompson [13].

To further investigate the characteristic features of QC, single surface trace analyses were made on six (6) facets to determine the angles formed by the oblong elements (see Fig. 1(a)). Since these elements form triangles, only two of the three angles (designated as A and B) for each triangle were measured and the third one (designated as C) was calculated from the other two. The results are given in Table 2, and show the average value of each angle to be about 60° . In addition, pairs of precisely matched micrographs were taken from mating fracture surfaces, as illustrated in Fig. 2. From Fig. 2, it can be seen that the geometrical markings are matched one-to-one across the mating fracture surfaces.

It is conceivable that these oblong elements correspond to the intersections of martensite laths with the local fracture surface, i.e., with the QC facet. The angles between these oblong elements would then correspond to angles between the traces of martensite laths or plates on the local fracture surface. Since the angles are approximately equal to 60° , it is reasonable to expect that quasi-cleavage occurred along specific crystallographic planes through martensite, and that the traces reflected the configuration of martensites with specific habit planes in prior-austenite.

3.2 Crystallographic Orientation of QC Facets

To investigate the possibility that cracking occurred along specific crystallographic planes through martensite, an etch-pit method was used to determine the crystallographic orientations of the facets [8,17]. For body-centered-cubic crystals, etch pits are produced on $\{100\}$ and $\{110\}$ planes and exhibit shapes as illustrated in Fig. 3(b). A typical example of etch pits on a QC facet is shown in Fig. 3(a). The hexagonal shape of the pits clearly shows that the QC facets correspond to $\{110\}_\alpha$ planes through the martensite. This result is consistent with the recent findings on iron single crystal and commercial alloy steels [6,8].

Based on this identification, the angles formed by the traces of martensite laths or plates on the $\{110\}_\alpha$ planes (i.e., the QC facets) can be readily determined if the habit planes of martensite are known. Information on martensite habit planes, however, is not available for AISI 4340 steel. Recent studies have shown that $\{111\}_\gamma$, $\{557\}_\gamma$ and $\{225\}_\gamma$ are possible habit planes of martensite in quenched and tempered, medium carbon and medium carbon-low alloy steels [19-21]. Calculations of angles formed by the traces of martensite laths or plates on $\{110\}_\alpha$ showed that the observed 60° arrangement could be satisfied by any of the three possible habit planes (see Appendix I). Another method is needed, therefore, to complete the identification of martensite habit planes in AISI 4340 steel.

4.0 DETERMINATION OF MARTENSITE HABIT PLANE IN AISI 4340 STEEL

Determinations of martensite habit planes in steels are usually made with the aid of retained austenite in the microstructure, which provides a link to the pre-transformation crystal structure, or by the use of two-surface trace analysis [22]. Direct determination of martensite habit planes for the steel used in this study, however, could not be made by the first method because no retained austenite was found. It was also difficult to use the two-surface trace analysis methods [22], because of the extreme difficulty in finding a prior-austenite grain that contained two distinctly different annealing twins. A method had to be developed, therefore, for selecting martensite habit planes from several candidates without requiring information from retained austenite or annealing twins. This method and its application to the analysis of AISI 4340 steel are described in the following subsections.

4.1 Principle of the Method

If $\{hkl\}_{\gamma}$ are the martensite habit planes for a metal A and the plane of a thin foil of this metal corresponds to a crystallographic plane $(uvw)_{\gamma}$ in its "prior-austenite" lattice, then the trace directions of $\{hkl\}_{\gamma}$ on $(uvw)_{\gamma}$ and the angles formed by these traces can be readily calculated by using the zone law and the corresponding direction cosines (see Appendix I). The results should be unique for a specific system of habit planes. Since martensite laths or plates lie in the habit planes, these traces and angles should correspond to those of martensite in the thin foil, i.e., in the $(uvw)_{\gamma}$ plane.

The $(uvw)_\gamma$ plane, however, is no longer accessible after the metal transforms completely from the parent austenite to the product martensite. Only the martensite planes that are parallel to the original plane $(uvw)_\gamma$ can be determined from selected area diffraction analysis of the transformed microstructure. Thus, if one can determine the original thin-foil plane, $(uvw)_\gamma$, in the "prior-austenite" lattice from these martensite planes, the martensite habit planes then can be determined from the measurements of angles between martensite traces on the thin foil. Such a transformation of martensite planes into its original austenite planes can be made by using the (M/A) matrices. These matrices can be derived from crystallographic relationships, such as the Kurdjumov-Sachs relationships [21,23], and recognize that martensite transformation involves shear deformation on a common slip plane in a given "prior-austenite" grain.

Because the analysis involves two or more martensite plates in a given foil and of the permissible freedom in indexing diffraction patterns, unique identification of a specific set of martensite habit planes requires the consideration of the crystallographic relationships between individual martensite plates in a given "prior-austenite" grain in the foil. The procedures for these analyses are outlined in the following subsection and are applied to the study of AISI 4340 steel subsequently.

4.2 Procedures

Based on the principles described above, the procedures for determining the martensite habit planes from candidate planes are as follows:

- (1) Find a region of the thin foil where three sets of martensite plates intersect to form triangles (for example, as in Fig. 4(a)).
- (2) Obtain selected area diffraction (SAD) patterns for each set of plates at a fixed foil orientation; usually perpendicular to the axis of the incident electron beam. (See Fig. 4(b), for example).
- (3) Determine the beam direction, or foil plane normal, relative to the martensite structure from the SAD pattern for each plate; i.e., determine the vector $\vec{B} = [xyz]_{\alpha'}$, which is normal to the $(xyz)_{\alpha'}$ plane.
- (4) Transform the $(xyz)_{\alpha'}$ plane to the corresponding $(uvw)_{\gamma}$ plane in "prior austenite" by using (M/A) matrices derived from the Kurdjumov-Sachs relationships for Fe-C alloys (see Appendix II).
- (5) Compute the angles between traces of candidate martensite habit planes on the $(uvw)_{\gamma}$ plane, and compare with measurements.
- (6) Select martensite habit planes from the candidate planes based on agreement with measurements.
- (7) Apply conditions of crystallographic constraint to obtain unique identification of martensite habit planes and their common plane in "prior-austenite".

It is expected that unique identification can be obtained from only two sets of martensite plates. Information from the third set would provide for confirmation of the analyses, and is not essential.

4.3 Results for AISI 4340 Steel

Three martensite plates, marked as I, II and III in Fig. 4(a), were chosen for analysis. It should be noted that the diffraction patterns obtained are imperfect, and contained spots from different zero-order Laue zones. An example of such an imperfect pattern, obtained from plate III, is shown in Fig. 7 with its indexing. The procedure outlined by Ryder and Pitsch [24] was followed in indexing these patterns.

The beam direction B for each plate of martensite was calculated by using the following relationship:

$$B = |g_1|^2(g_2 \wedge g_3) + |g_2|^2(g_3 \wedge g_1) + |g_3|^2(g_1 \wedge g_2) \quad (1)$$

The vectors g_1 , g_2 and g_3 are three reciprocal vectors, which correspond to strong reflections (or bright spots) in the SAD pattern, and do not all lie in the same zone. The beam directions for martensite plates I, II and III were found to be $[\bar{4} \bar{3} 1]_\alpha$, $[\bar{6} 4 \bar{1}]_\alpha$, and $[\bar{1} 1.2 2.3]_\alpha$, respectively. These beam directions represent the normals of the $(\bar{4} \bar{3} 1)_\alpha$, $(\bar{6} 4 \bar{1})_\alpha$, and $(\bar{1} 1.2 2.3)_\alpha$ martensite planes for each of the plates, which are parallel to the foil plane. It should be noted that the indices refer to the coordinate system chosen for each of the plates, and their relationships are to be established subsequently.

The $(xyz)_\alpha$ plane for each martensite plate was then transformed into its corresponding $(uvw)_\gamma$ plane in "prior-austenite" by using the appropriate (M/A) matrix (see Appendix II). The equation for the transformation may be expressed compactly as follows:

$$(u \ v \ w)_\gamma = (x \ y \ z)_\alpha (M/A) \quad (2)$$

(M/A) is the correspondence matrix.

As a first step, all twenty-four (24) correspondence matrices (Appendix II) were used for identifying all of the possible planes in the "prior-austenite" lattice that would correspond to the $(xyz)_\alpha$ foil plane in martensite. A total of 72 planes were identified, 12 of each of 2 types for each of the martensite plates (see Table 3). Angles formed by the traces of candidate martensite habit planes (namely, the $\{111\}_\gamma$, $\{557\}_\gamma$ and $\{225\}_\gamma$) on each of these planes were then computed and compared with the measured angles. The comparison (see Table 4) shows that only the $\{225\}_\gamma$ planes provided agreement with the experimentally observed angles, and identifies these planes as the martensite habit planes in this AISI 4340 steel.

In addition, the potential common planes are reduced to 3 groups of 3 planes each (Table 4). The grouping reflects the recognition that there should be only one common plane (the foil plane) for the martensites in the "prior austenite" lattice. Indeed, each of the group should be viewed as a single common plane, with the misorientations of planes within each group reflecting the accuracy of SAD analyses. The indicated misorien-

tation, for example, between $(335)_\gamma$ and $(547)_\gamma$ is about 4.7° , and that between $(1.2 \ 1.3 \ 3.3)_\gamma$ for plate III and the other two is about 12° . The larger error is attributable to the thinness of foil in this region and the attendant error in defining plane normal from SAD analysis [25], and is nevertheless acceptable. Within the indicated error, the common plane is considered to be one of the $\{335\}_\gamma$ planes given in Table 5.

Final selection of one of the $\{335\}_\gamma$ planes as the common plane and of the associated correspondence matrices was made by considering the directions of martensites in the thin foil (bright field image) in relation to the SAD patterns. Using martensite plates I and II (Fig. 4(a)), the calculated traces of martensites for the $(335)_\gamma$ plane (namely, $[\bar{1} \ 0.4 \ 7]_\alpha$ and $[1 \ \bar{1} \ 1]_\alpha$) provided the closest agreement with observations.

One may conclude, therefore, that the martensite habit planes in the AISI 4340 steel used in this study are the $\{225\}_\gamma$ planes. The foil plane in which martensites appear as triads with approximately 60° included angles has been identified as $(335)_\gamma$. Since this plane is close to $(110)_\alpha$, the consistency between the observed configuration of martensites in the thin foil and that of the oblong elements on the quasi-cleavage facets provides further confirmation of the nature of quasi-cleavage in this steel.

5.0 DISCUSSIONS

This study has shown that quasi-cleavage produced by hydrogen assisted cracking in AISI 4340 steel occurred on planes parallel to $\{110\}_\alpha$ in the martensite lattice. Similar results

were reported recently for internal hydrogen embrittlement in pure iron and in other steels [1-8]. It was suggested that slip planes can act, under stress, as hydrogen accumulation sites, and that cracking can occur as a result of the interaction between hydrogen and the slip structure (e.g., slip bands or cells) [6,8]. This interpretation may apply also to the case of quasi-cleavage.

Quasi-cleavage, however, is not always an important fracture mode. For example, only small amounts of quasi-cleavage were observed in the AISI 4340 steels [14-16]. For specimens tested in hydrogen at 133kPa and 270K, QC amounted to about 14 ± 7 pct (estimated 95 pct confidence interval) of the fracture surface. The predominant component was cracking along the prior-austenite grain boundaries. Thus, it appears that quasi-cleavage would occur only when no favorably oriented prior-austenite grain boundaries are available.

Although the principal morphology of quasi-cleavage is as described, there are a few exceptions. Some QC facets do not show discernible geometrical markings, and some others exhibit markings at angles that differ significantly from 60° . These minor exceptions may be caused by concomitant ductile tearing, which obscured the geometrical markings in the first case, and by having the QC facets oriented at large angles with respect to the macroscopic crack plane in others. An example for the latter case is given by QC facet 2-2' in Fig. 2.

In principle, the proposed method for determining martensite habit planes can be used without foreknowledge of the candidate habit planes, because the geometrical relationship between

martensite traces on a flat thin foil is unique for a specific habit plane system. In this case, very precise determinations of beam directions and precise trace analyses would be required.

6.0 SUMMARY

In this study, the crystallographic features of quasi-cleavage produced by sustained-load crack growth in AISI 4340 steel, exposed to hydrogen and to hydrogen sulfide, have been examined. A method has been proposed for determining the martensite habit planes without the need for concomitant presence of retained austenite or annealing twins in the martensitic microstructure. The results showed that quasi-cleavage occurred along $\{110\}_\alpha$ planes through martensites. The habit planes of martensites have been separately identified as $\{225\}_\gamma$. Markings on the QC facets have been shown to be consistent with cracking along $\{110\}_\alpha$ through martensites with $\{225\}_\gamma$ habit planes.

ACKNOWLEDGEMENT

This work was supported in part by the Office of Naval Research under Contract N00014-75-C-0543, NR 036-097. Helpful discussions with Dr. A. Marder of the Homer Research Laboratory, Bethlehem Steel Corporation is gratefully acknowledged.

APPENDIX I

Angles Formed by Traces of Martensite Laths on $(11\bar{0})_{\alpha}$,

The intersections of martensite laths or plates with the $(111)_{\gamma}$ plane produce traces on this plane which would have the same angular relationships as those on the corresponding $(11\bar{0})_{\alpha}$ plane in the martensite lattice. The angular relationships between these traces can be readily determined by using the zone law and the corresponding direction cosines (i.e., dot-product of two vectors).

$$\underline{a} = a_1 \underline{i} + a_2 \underline{j} + a_3 \underline{k} = \begin{vmatrix} \underline{i} & \underline{j} & \underline{k} \\ h & k & l \\ u & v & w \end{vmatrix} \quad (I-1)$$

$$\underline{b} = b_1 \underline{i} + b_2 \underline{j} + b_3 \underline{k} = \begin{vmatrix} \underline{i} & \underline{j} & \underline{k} \\ h & k & l \\ u' & v' & w' \end{vmatrix} \quad (I-2)$$

$$\cos\theta = \underline{a} \cdot \underline{b} / (|\underline{a}| |\underline{b}|) \quad (I-3)*$$

The vectors \underline{a} and \underline{b} are the intersections of $(u \ v \ w)$ and $(u' \ v' \ w')$ planes with $(h \ k \ l)$ plane respectively. The angle θ is formed by \underline{a} and \underline{b} .

The intersections of $\{111\}_{\gamma}$ martensite laths with the $(111)_{\gamma}$ plane have been determined and are listed in Table I-1.

*For iron-carbon alloys containing less than 0.6 pct carbon, it is reasonable to ignore the tetragonality of the martensite lattice [24,25].

Table I-1

Traces of Martensite with $\{111\}_{\gamma}$ Habit Planes on $(111)_{\gamma}$

Habit Plane	Trace on $(111)_{\gamma}$
$(11\bar{1})_{\gamma}$	$[\bar{1}10]_{\gamma}$
$(1\bar{1}1)_{\gamma}$	$[\bar{1}01]_{\gamma}$
$(\bar{1}11)_{\gamma}$	$[0\bar{1}1]_{\gamma}$

Obviously, these traces form 60° angles with respect to each other.

For $\{225\}_{\gamma}$ and $\{557\}_{\gamma}$ habit planes, the martensite laths do intersect with $(111)_{\gamma}$ and produce traces that also form 60° angles with respect to each other (see Table I-2).

Table I-2

Traces of Martensite with $\{225\}_{\gamma}$ and $\{557\}_{\gamma}$ Habit Planes on $(111)_{\gamma}$

Habit Planes	Trace on $(111)_{\gamma}$
$(225)_{\gamma}, (22\bar{5})_{\gamma}$	$[\bar{1}10]_{\gamma}$
$(252)_{\gamma}, (2\bar{5}2)_{\gamma}$	$[10\bar{1}]_{\gamma}$
$(522)_{\gamma}, (5\bar{2}2)_{\gamma}$	$[01\bar{1}]_{\gamma}$
$(557)_{\gamma}, (55\bar{7})_{\gamma}$	$[\bar{1}10]_{\gamma}$
$(575)_{\gamma}, (5\bar{7}5)_{\gamma}$	$[10\bar{1}]_{\gamma}$
$(755)_{\gamma}, (7\bar{5}5)_{\gamma}$	$[01\bar{1}]_{\gamma}$

The $(22\bar{5})_{\gamma}$, $(2\bar{5}2)_{\gamma}$ and $(\bar{5}22)_{\gamma}$ planes are oriented at 96° with respect to $(111)_{\gamma}$ and are the more likely habit planes associated with shearing deformation in $(111)_{\gamma}$. The $(225)_{\gamma}$, $(252)_{\gamma}$ and $(522)_{\gamma}$ form angles of approximately 25° with $(111)_{\gamma}$, and are not considered to be the likely habit planes for shearing on $(111)_{\gamma}$. Similarly $(55\bar{7})_{\gamma}$, $(5\bar{7}5)_{\gamma}$ and $(\bar{7}55)_{\gamma}$ are oriented at 80° with respect to $(111)_{\gamma}$ and are considered to be likely habit planes; while the others are not.

APPENDIX II

Lattice Correspondence between Austenite and Martensite

To transform the $(uvw)_\alpha$ plane in martensite into its corresponding $(hkl)_\gamma$ plane in the "prior-austenite", one needs to establish the correspondence matrix (M/A) for the transformation. Following the method of Jaswan and Wheeler [26], based on analytical geometry, the lattice correspondence matrix can be established from the relative orientation between austenite and martensite.

For the case of iron-carbon alloys, the relative orientation between austenite and martensite is described by the set of Kurdjumov-Sachs relationships [21,23]. Since there are twenty-four (24) variants of the Kurdjumov-Sachs relationships, a total of 24 correspondence matrices needs to be established and examined. These matrices are given in Table II-1.

The specific lattice correspondence matrices that operate in the transformation may be selected in accordance with (i) the specific variants of Kurdjumov-Sachs relationships that are known or are given, and (ii) the conditions of constraint for the differently oriented martensite laths or plates within a single "prior-austenite" grain. The conditions of constraint are imposed to ensure that the foil normals for the martensite laths or plates are compatible with one another. In other words, because the martensites are in the same foil and are contained within one "prior-austenite" grain, the foil normals deduced from them must correspond or transform to the same foil normal in the corresponding "prior-austenite" lattice.

Table II-1
Lattice Correspondence Matrices (M/A)

No.	Variant	Matrix	No.	Variant	Matrix
1.	(111)[011]	$\begin{pmatrix} \bar{1} & 1 & 0 \\ 1 & 1 & 0 \\ 0 & 0 & 1 \end{pmatrix}$	2.	(111)[011]	$\begin{pmatrix} 1 & \bar{1} & 0 \\ 0 & 0 & 1 \\ 1 & 1 & 0 \end{pmatrix}$
3.	(111)[110]	$\begin{pmatrix} 1 & 0 & \bar{1} \\ 1 & 0 & 1 \\ 0 & 1 & 0 \end{pmatrix}$	4.	(111)[110]	$\begin{pmatrix} \bar{1} & 0 & 1 \\ 0 & 1 & 0 \\ 1 & 0 & 1 \end{pmatrix}$
5.	(111)[101]	$\begin{pmatrix} 0 & \bar{1} & 1 \\ 0 & 1 & 1 \\ 1 & 0 & 0 \end{pmatrix}$	6.	(111)[101]	$\begin{pmatrix} 0 & 1 & \bar{1} \\ 1 & 0 & 0 \\ 0 & 1 & 1 \end{pmatrix}$
7.	(111)[110]	$\begin{pmatrix} 1 & 0 & 1 \\ 1 & 0 & \bar{1} \\ 0 & 1 & 0 \end{pmatrix}$	8.	(111)[110]	$\begin{pmatrix} \bar{1} & 0 & \bar{1} \\ 0 & 1 & 0 \\ 1 & 0 & \bar{1} \end{pmatrix}$
9.	(111)[101]	$\begin{pmatrix} \bar{1} & 1 & 0 \\ 0 & 0 & \bar{1} \\ 1 & 1 & 0 \end{pmatrix}$	10.	(111)[101]	$\begin{pmatrix} 1 & \bar{1} & 0 \\ 1 & 1 & 0 \\ 0 & 0 & \bar{1} \end{pmatrix}$
11.	(111)[011]	$\begin{pmatrix} \bar{1} & 0 & \bar{1} \\ 1 & 0 & \bar{1} \\ 0 & 1 & 0 \end{pmatrix}$	12.	(111)[011]	$\begin{pmatrix} 1 & 0 & 1 \\ 0 & 1 & 0 \\ 1 & 0 & \bar{1} \end{pmatrix}$
13.	(111)[101]	$\begin{pmatrix} \bar{1} & \bar{1} & 0 \\ 0 & 0 & 1 \\ 1 & \bar{1} & 0 \end{pmatrix}$	14.	(111)[101]	$\begin{pmatrix} 1 & 1 & 0 \\ 1 & \bar{1} & 0 \\ 0 & 0 & 1 \end{pmatrix}$
15.	(111)[110]	$\begin{pmatrix} 0 & \bar{1} & \bar{1} \\ 0 & 1 & 1 \\ 1 & 0 & 0 \end{pmatrix}$	16.	(111)[110]	$\begin{pmatrix} 0 & 1 & 1 \\ 1 & 0 & 0 \\ 0 & \bar{1} & 1 \end{pmatrix}$
17.	(111)[011]	$\begin{pmatrix} 1 & 0 & \bar{1} \\ 0 & \bar{1} & 0 \\ 1 & 0 & 1 \end{pmatrix}$	18.	(111)[011]	$\begin{pmatrix} \bar{1} & 0 & 1 \\ 1 & 0 & 1 \\ 0 & \bar{1} & 0 \end{pmatrix}$
19.	(111)[011]	$\begin{pmatrix} \bar{1} & 0 & \bar{1} \\ 0 & 1 & 0 \\ \bar{1} & 0 & 1 \end{pmatrix}$	20.	(111)[011]	$\begin{pmatrix} 1 & 0 & 1 \\ \bar{1} & 0 & 1 \\ 0 & 1 & 0 \end{pmatrix}$
21.	(111)[101]	$\begin{pmatrix} \bar{1} & \bar{1} & 0 \\ 1 & 1 & 0 \\ 0 & 0 & 1 \end{pmatrix}$	22.	(111)[101]	$\begin{pmatrix} 1 & 1 & 0 \\ 0 & 0 & 1 \\ \bar{1} & 1 & 0 \end{pmatrix}$
23.	(111)[110]	$\begin{pmatrix} 0 & \bar{1} & 1 \\ \bar{1} & 0 & 0 \\ 0 & 1 & 1 \end{pmatrix}$	24.	(111)[110]	$\begin{pmatrix} 0 & 1 & \bar{1} \\ 0 & 1 & 1 \\ \bar{1} & 0 & 0 \end{pmatrix}$

REFERENCES

1. I. M. Bernstein: Met. Trans., 1 (1970), p. 3143.
2. F. Terasaki and F. Nakasato: in Proc. of Conf. on mechanism of delayed fracture caused by hydrogen, Tokyo (1975), p. 165.
3. F. Nakasato and I. M. Bernstein: Met. Trans., 9A (1978), p. 1317.
4. H. Takahashi, T. Takeyama and T. Hara: Nihon-Kinzoku Gakkaishi, 43 (1979), p. 492.
5. A. Inone, Y. Hosoya and T. Masumoto: Tetsu-to-Hagane, 65 (1979), p. 5.
6. Shigeharu Hinotani, Fukunaga Terasak and Fukukazu Nakasato: in Proceedings JIMIS-2, Hydrogen in Metals (1980), Tokyo, p. 421.
7. T. Takeyama and H. Takahashi: in Proceedings JIMIS-2, Hydrogen in Metals (1980), Tyoko, p. 409.
8. Takao Araki and Yoneo Kikuta: in Proceedings JIMIS-2, Hydrogen in Metals (1980), Tokyo, p. 425.
9. A. W. Thompson: in Environment Degradation of Engineering Materials, M. R. Louthan and R. P. McNitt, eds., VPI Press, Blacksburg, VA (1977), pp. 3-17.
10. A. W. Thompson and I. M. Bernstein: in Fracture, 2, D. Taplin, ed., Univ. of Waterloo Press, Waterloo, Ont. (1977), pp. 249-54.
11. A. W. Thompson and I. M. Bernstein: in Hydrogen in Metals, (Paris) 3, Paper 3A-6, Pergamon Press, New York (1977).
12. A. W. Thompson and I. M. Bernstein: in Hydrogen Effects in Metals, The Met. Society of AIME press, New York (1981), p. 291.
13. J. E. Costa and A. W. Thompson: Met. Trans., 12A (1980), p. 761.
14. G. W. Simmons, P. S. Pao and R. P. Wei: Met. Trans., 9A (1978), pp. 1147-1158.
15. M. Lu, P. S. Pao, N. H. Chan, K. Klier and R. P. Wei: in Proceedings JIMIS-2, Hydrogen in Metals (1980) Tyoko, p. 449.
16. M. Lu, P. S. Pao, T. W. Weir, G. W. Simmons and R. P. Wei: Met. Trans., 12A (1981), p. 805.
17. T. Taoka, F. Furubayashi, and S. Takench: Japanese Journal of Applied Physics, 4, (1965) p. 120.
18. Metals Handbook, 8, 8th Edition, ASM (1973), p. 69.
19. J. S. Bowles: Acta Crystallographic, 4 (1951), p. 162.

20. A. R. Marder and G. R. Krauss, Trans. ASM, 62 (1969), p. 947.
21. C. M. Wayman: in Introduction to the Crystallography of Martensite Transformation, the MacMillan Company, New York, p. 153.
22. A. H. Greninger and A. R. Troiano: Trans. AIME, 140 (1940), p. 307.
23. G. Kurdjumov and G. Sachs: Z. Phys., 64 (1930), p. 325.
24. P. L. Ryder and W. Pitsch: Phil. Mag., 18 (1968), p. 807.
25. C. Laird, E. Eichen and W. R. Bitler: J. Appl. Phys., 37 (1966), p. 2225.
26. M. A. Jaswan and J. A. Wheeler: Acta Crystallographica, 1 (1948), p. 10.

TABLE 1

CHEMICAL COMPOSITION, HEAT TREATMENT, AND ROOM TEMPERATURE
TENSILE PROPERTIES OF THE AISI 4340 STEEL INVESTIGATED

<u>Chemical Composition (Weight Percent)</u>									
C	Mn	P	S	Si	Ni	Cr	Mo	Co	Ti
0.42	0.70	0.0009	0.0012	0.28	1.83	0.79	0.24	0.011	<0.005

Heat Treatment

Normalize, 1 h, 900°C, A.C. + austenitize, 1 h, 843°C, O.Q. + temper,
1 h, 204°C, A.C.

A.C. = air cool; O. Q. = oil quench

Tensile Properties

0.2% Offset Yield Strength MPa	Tensile Strength MPa	Young's Modulus GPa	Elongation Pct
1344	2082	201	9
			(in 3.56 cm)

TABLE 2
Angles Between Microstructural Elements

Photo No.	Angle A	Angle B	Angle C
1	60	64	56
2	61	63	56
3	61	63	56
4	61	63	56
5	60	62	58
6	61	-	-
Average	60.6	63.0	56.4

From scanning electron fractographs

TABLE 3

Twenty-four possible foil planes in the "prior-austenite" lattice for each $(x\ y\ z)_\alpha$, foil plane in martensite

Foil Plane in Martensite Lattice	$(\bar{4}\bar{3}1)_\alpha$	$(\bar{6}4\bar{1})_\alpha$	$(\bar{1}\ 1.2\ 2.3)_\alpha$
Foil plane in "prior-austenite" lattice*	$\{335\}_\gamma$ $\{117\}_\gamma$	$\{547\}_\gamma$ $\{2\ 1\ 10\}_\gamma$	$\{1.3\ 1.2\ 3.3\}_\gamma$ $\{2.2\ 0.2\ 2.3\}_\gamma$

* 12 possible planes for each class of planes indicated. The specific planes may be determined through the use of (M/A) matrices and the Kurdjumov-Sachs relations (see Appendix II).

TABLE 4

Calculated Angles Between Martensite Plates on $(u \ v \ w)_{\gamma}$

Potential Common Planes From Martensite Plate		Angle	Candidate Habit Planes		
			$\{111\}_{\gamma}$	$\{557\}_{\gamma}$	$\{225\}_{\gamma}$
I	$(335)_{\gamma}$	A	65	63	61.5
	$(353)_{\gamma}$	B	65	63	59.5
	$(533)_{\gamma}$	C	50	54	59
II	$(547)_{\gamma}$	A	66	63	61.1
	$(574)_{\gamma}$	B	63	62	60.8
	$(745)_{\gamma}$	C	51	55	58.1
III	$(1.2 \ 1.3 \ 3.3)_{\gamma}$	A	71.3	62	60.8
	$(1.3 \ 3.3 \ 1.2)_{\gamma}$	B	71.3	59.8	59.8
	$(3.3 \ 1.2 \ 1.3)_{\gamma}$	C	37.4	58.2	59.4

Measured Angles: A = 63°, B = 59° and C = 58°

TABLE 5

The Specific Correspondence Matrix and the
20 Corresponding $(u \ v \ w)_{\gamma}$ For Each $(x \ y \ z)_{\alpha}$,

Martensite Plate	I	II	III
Plane in Martensite	$(\bar{4} \ \bar{3} \ 1)_{\alpha}$	$(\bar{6} \ 4 \ \bar{1})_{\alpha}$	$(\bar{1} \ 1.2 \ 2.3)_{\alpha}$
(M/A) Matrix	$\begin{pmatrix} 1 & 0 & 1 \\ 0 & 1 & 0 \\ 1 & 1 & \bar{1} \end{pmatrix}$	$\begin{pmatrix} \bar{1} & 0 & \bar{1} \\ 0 & 1 & 0 \\ 1 & 0 & \bar{1} \end{pmatrix}$	$\begin{pmatrix} 0 & 1 & \bar{1} \\ 1 & 0 & 0 \\ 0 & 1 & 1 \end{pmatrix}$
Corresponding Plane in "Prior" Austenite	$(335)_{\gamma}$	$(547)_{\gamma}$	$(1.2 \ 1.3 \ 3.3)_{\gamma}$
Deviation From $(335)_{\gamma}$	0	4.7	$12^{\circ*}$

* Large deviation caused in part by error in the calculated beam direction, the error being introduced by thinness of the foil in this region.

FIGURE CAPTIONS

- Fig. 1: SEM micrographs of (a) QC facet and (b) martensite structure.
- Fig. 2: SEM micrographs of QC facets on mating fracture surfaces.
- Fig. 3: (a) SEM micrograph of etch-pits on a QC facet, and (b) sketches of the pit shape on {100} and {110} plane in a b.c.c. crystal.
- Fig. 4: Transmission electron micrographs of intersecting martensite plates.
- Fig. 5: Selected area diffraction pattern for martensite plate I (in Fig. 4) and its indices.
- Fig. 6: Selected area diffraction pattern for martensite plate II (in Fig. 4) and its indices.
- Fig. 7: Selected area diffraction pattern for martensite plate III (in Fig. 4) and its indices.

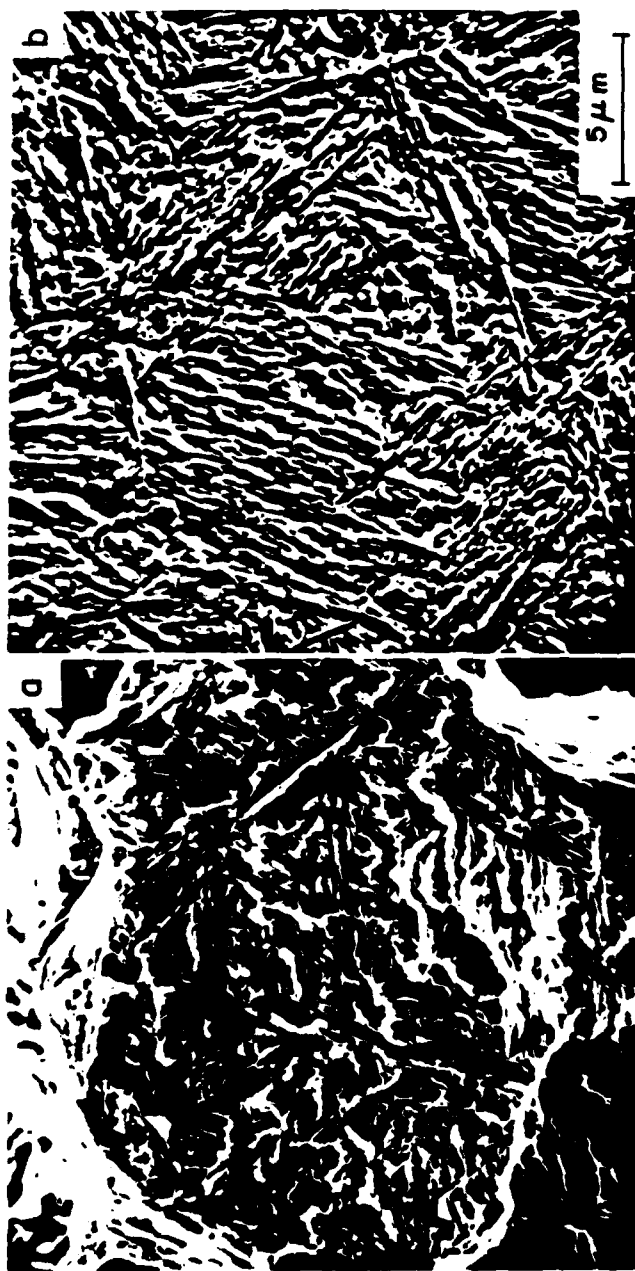


Fig. 1: SEM micrographs of (a) QC facet and (b) martensite structure.

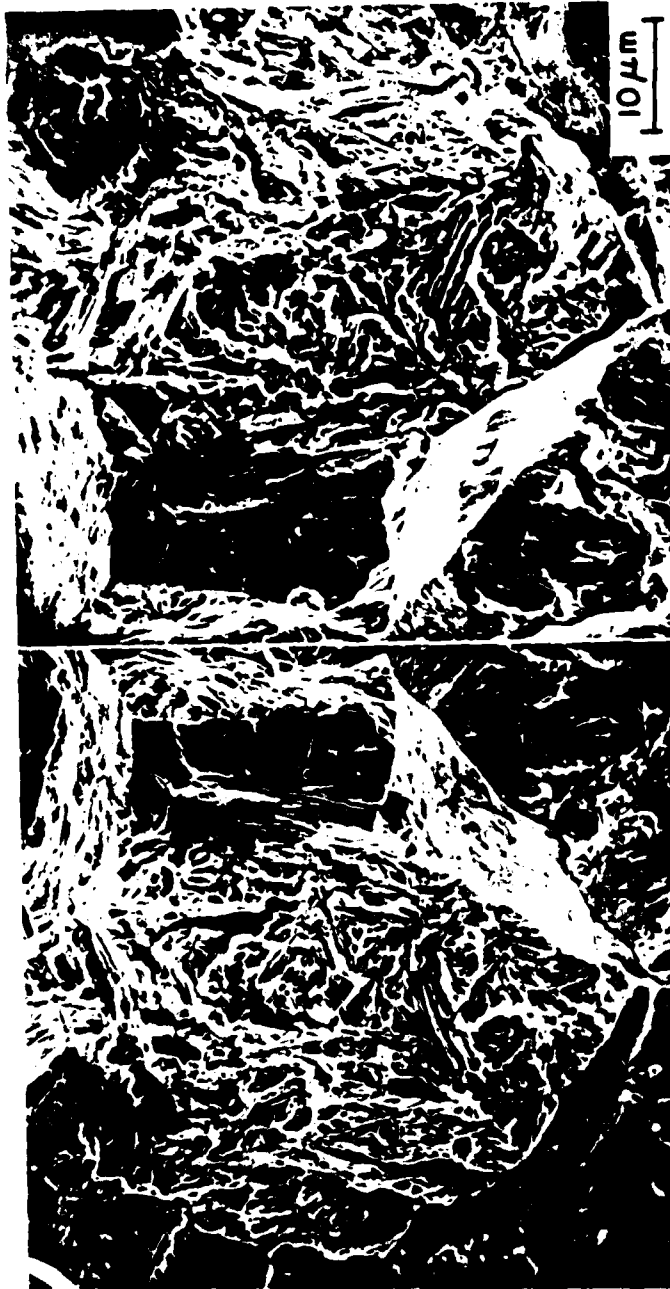


Fig. 2: SEM micrographs of QC facets on mating fracture surfaces.

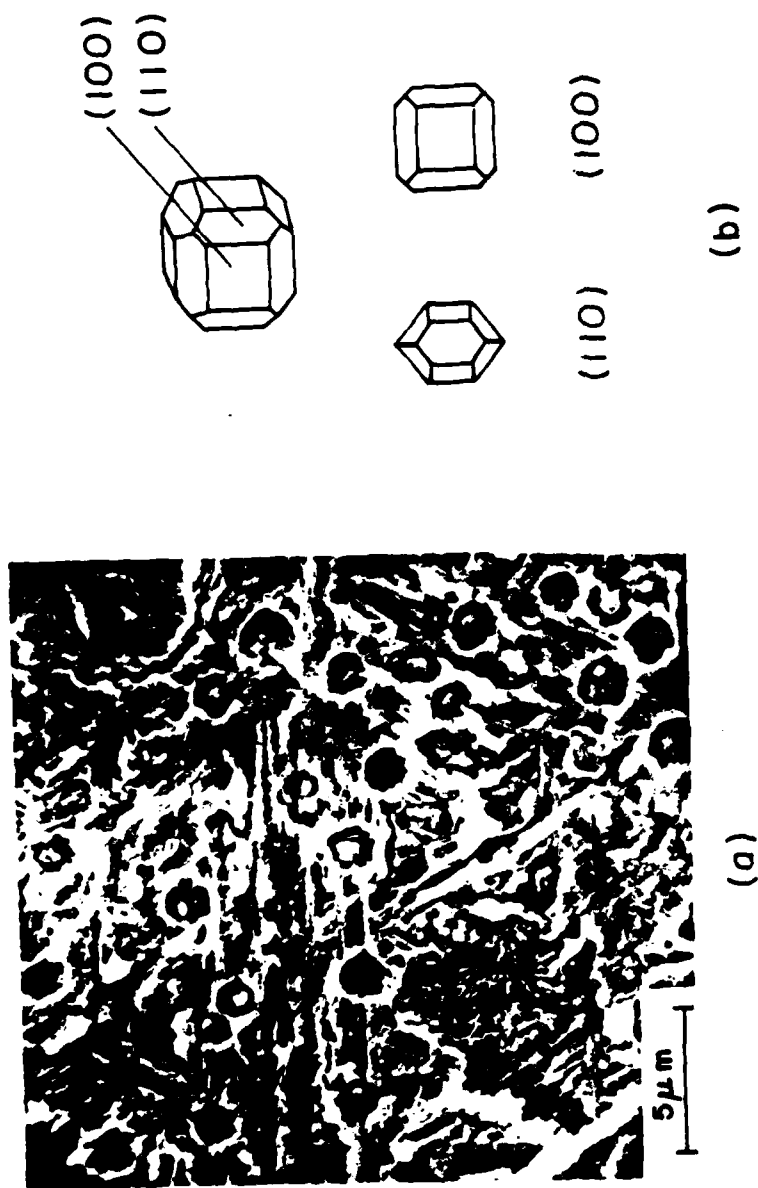


Fig. 3: (a) SEM micrograph of etch-pits on a QC facet, and (b) sketches of the pit shape on $\{100\}$ and $\{110\}$ plane in a b.c.c. crystal.

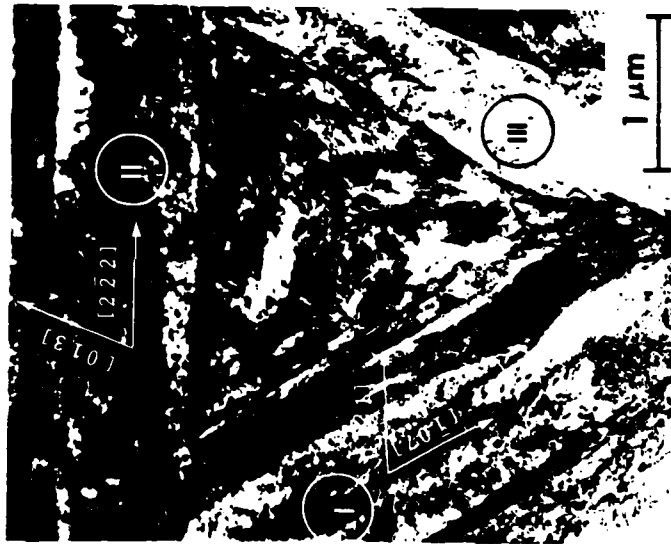


Fig. 4: Transmission electron micrographs of intersecting martensite plates.

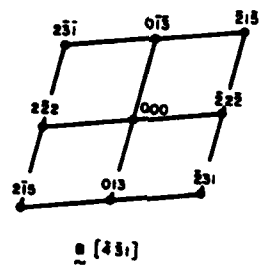
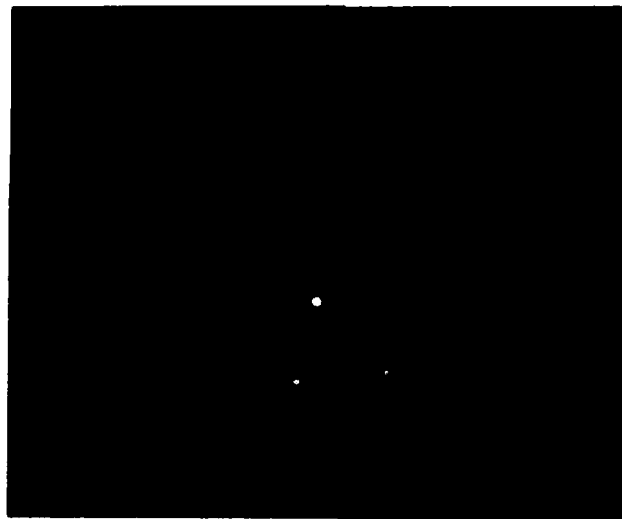


Fig. 5: Selected area diffraction pattern for martensite plate I (in Fig. 4) and its indices.

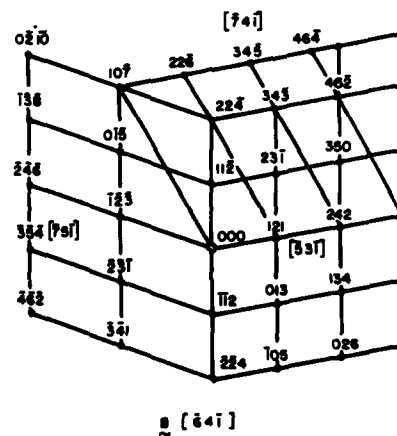
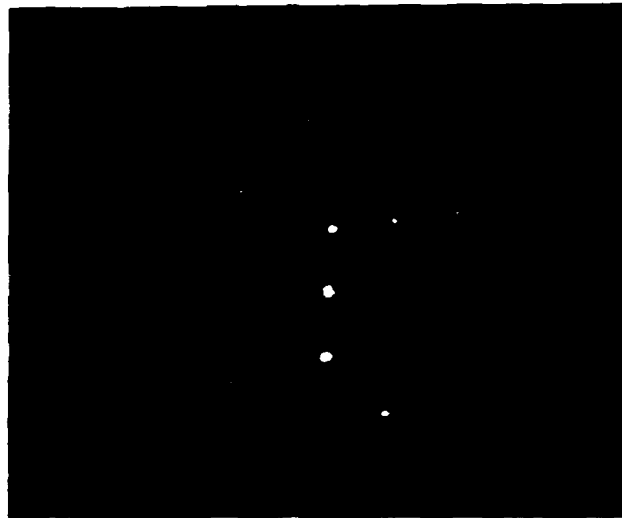


Fig. 6: Selected area diffraction pattern for martensite plate II (in Fig. 4) and its indices.

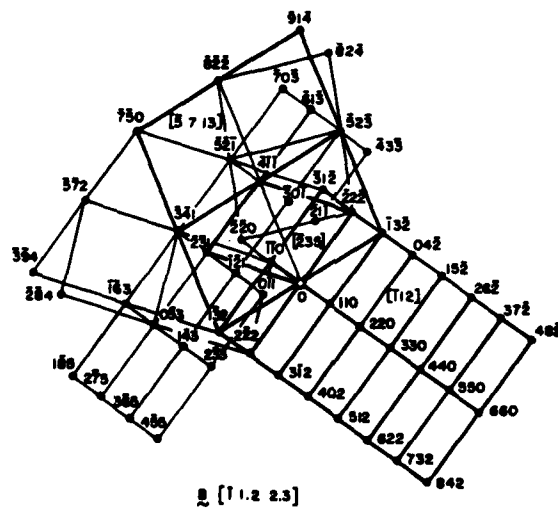


Fig. 7: Selected area diffraction pattern for martensite plate III (in Fig. 4) and its indices.

BASIC DISTRIBUTION LIST

Technical and Summary Reports

April 1978

<u>Organization</u>	<u>Copies</u>	<u>Organization</u>	<u>Copies</u>
Defense Documentation Center Cameron Station Alexandria, VA 22314	12	Naval Air Propulsion Test Center Trenton, NJ 08628 ATTN: Library	1
Office of Naval Research Department of the Navy 800 N. Quincy Street Arlington, VA 22217		Naval Construction Battalion Civil Engineering Laboratory Port Hueneme, CA 93043 ATTN: Materials Division	1
ATTN: Code 471	1	Naval Electronics Laboratory San Diego, CA 92152	
Code 102	1	ATTN: Electron Materials Sciences Division	1
Code 470	1		
Commanding Officer Office of Naval Research Branch Office Building 114, Section D 666 Summer Street Boston, MA 02210	1	Naval Missile Center Materials Consultant Code 3312-1 Point Mugu, CA 92041	1
Commanding Officer Office of Naval Research Branch Office 536 South Clark Street Chicago, IL 60605	1	Commanding Officer Naval Surface Weapons Center White Oak Laboratory Silver Spring, MD 20910 ATTN: Library	1
Office of Naval Research San Francisco Area Office One Hallidie Plaza Suite 601 San Francisco, CA 94102	1	David W. Taylor Naval Ship Research and Development Center Materials Department Annapolis, MD 21402	1
Naval Research Laboratory Washington, DC 20375		Naval Undersea Center San Diego, CA 92132 ATTN: Library	1
ATTN: Codes 6000	1	Naval Underwater System Center Newport, RI 02840	
6100	1	ATTN: Library	1
6300	1		
6400	1	Naval Weapons Center China Lake, CA 93555	
2627	1	ATTN: Library	1
Naval Air Development Center Code 382 Warminster, PA 18964		Naval Postgraduate School Monterey, CA 93940	
ATTN: Mr. F. S. Williams	1	ATTN: Mechanical Engineering Department	1

BASIC DISTRIBUTION LIST (cont'd)

<u>Organization</u>	<u>Copies</u>	<u>Organization</u>	<u>Copies</u>
Naval Air Systems Command Washington, DC 20360 ATTN: Codes 52031 52032	1	NASA Headquarters Washington, DC 20546 ATTN: Code:RRM	1
Naval Sea System Command Washington, DC 20362 ATTN: Code 035	1	NASA Lewis Research Center 21000 Brookpark Road Cleveland, OH 44135 ATTN: Library	1
Naval Facilities Engineering Command Alexandria, VA 22331 ATTN: Code 03	1	National Bureau of Standards Washington, DC 20234 ATTN: Metallurgy Division Inorganic Materials Div.	1 1
Scientific Advisor Commandant of the Marine Corps Washington, DC 20380 ATTN: Code AX	1	Director Applied Physics Laboratory University of Washington 1013 Northeast Forthieth Street Seattle, WA 98105	1
Naval Ship Engineering Center Department of the Navy Washington, DC 20360 ATTN: Code 6101	1	Defense Metals and Ceramics Information Center Battelle Memorial Institute 505 King Avenue Columbus, OH 43201	1
Army Research Office P.O. Box 12211 Triangle Park, NC 27709 ATTN: Metallurgy & Ceramics Program	1	Metals and Ceramics Division Oak Ridge National Laboratory P.O. Box X Oak Ridge, TN 37380	1
Army Materials and Mechanics Research Center Watertown, MA 02172 ATTN: Research Programs Office	1	Los Alamos Scientific Laboratory P.O. Box 1663 Los Alamos, NM 87544 ATTN: Report Librarian	1
Air Force Office of Scientific Research Bldg. 410 Bolling Air Force Base Washington, DC 20332 ATTN: Chemical Science Directorate Electronics & Solid State Sciences Directorate	1 1	Argonne National Laboratory Metallurgy Division P.O. Box 229 Lemont, IL 60439	1
Air Force Materials Laboratory Wright-Patterson AFB Dayton, OH 45433	1	Brookhaven National Laboratory Technical Information Division Upton, Long Island New York 11973 ATTN: Research Library	1
Library Building 50, Rm 134 Lawrence Radiation Laboratory Berkeley, CA	1	Office of Naval Research Branch Office 1030 East Green Street Pasadena, CA 91106	1

16 November 1981

DISTRIBUTION LIST
Corrosion Mechanisms

Professor J. P. Hirth
Ohio State University
Department of Metallurgical Engineering
1314 Kinnear Road
Columbus, OH 43212

Dr. J. Kruger
National Bureau of Standards
Washington, DC 20234

Dr. H. K. Birnbaum
University of Illinois
Department of Metallurgy and Mining Engineering
Urbana, IL 61801

Dr. D. J. Duquette
Rensselaer Polytechnic Institute
Department of Metallurgical Engineering
Troy, NY 12181

Dr. R. P. Wei
Lehigh University
Institute for Fracture and Solid Mechanics.
Bethlehem, PA 18015

Prof. H. W. Pickering
Pennsylvania State University
Department of Material Science
University Park, PA 16802

Prof. I. M. Bernstein
Carnegi-Mellon University
Schenley Park
Pittsburg, PA 15213

Dr. T. R. Beck
Electrochemical Technology Corporation
10035 31st Avenue, N.E.
Seattle, WA 98125

Prof. R. T. Foley
The American University
Washington, DC 20016

Dr. D. L. Davidson
Southwest Research Institute
8500 Culebra Road
P.O. Box Drawer 28510
San Antonio, TX 78284

Dr. Barry C. Syrett
Stanford Research Institute
333 Ravenswood Avenue
Menlo Park, CA 94025

Prof. S. Weissmann
Rutgers, The State University
of New Jersey
College of Engineering
New Brunswick, NY 08903

Prof. H. Herman
State University of New York
Material Science Department
Stony Brook, NY 11794

Prof. R. M. Latanision
Massachusetts Institute of
Technology
77 Massachusetts Avenue, Room E19-702
Cambridge, MA 02139

Prof. E. A. Starke, Jr.
Dept. of Materials Science
University of Virginia
Charlottesville, VA 22901

Prof. Morris E. Fine
Northwestern University
The Technological Institute
Evanston, IL 60201

Dr. C. S. Kortovich
TRW, Inc.
2355 Euclid Avenue
Cleveland, OH 44117

Dr. O. Buck
Rockwell International Science Center
1049 Camino Dos Rios
P.O. Box 1085
Thousand Oaks, CA 91360

Dr. R. J. Arsenault
University of Maryland
College Park, MD 20742

Dr. F. Mansfeld
Rockwell International (Science Ctr)
1049 Camino Dos Rios
P.O. Box 1085
Thousand Oaks, CA 91360

Continue of Distribution List

036
16 November 198

Dr. Paul Gordon
Illinois Institute of Technology
Department of Metallurgical and Materials
Engineering
Chicago, IL 60616

Dr. Theodore R. Beck
Electrochemical Technology Corp
3935 Leary Way NW
Seattle, Washington 98107

Dr. H. Leidheiser, Jr.
Lehigh University
Bethlehem, PA 18015

Dr. J. V. McArdle
University of Maryland
College Park, MD 20742

Br. E. McCafferty
Naval Research Laboratory
Washington, DC 20375

Prof. J. G. Byrne
The University of Utah
Dept. of Materials Science & Engineering
Salt Lake City, Utah 84112

Prof. A. J. Ardell
University of California
School of Engineering and Applied Science
405 Hilgard Ave.
Los Angeles, CA 90024

Prof. J. A. S. Green
Martin Marietta Corporation
1450 South Rolling Road
Baltimore, MD 21227

Prof. G.H. Meier & F.S. Pettit
University of Pittsburgh
Dept. of Metallurgical and Materials
Engineering
Pittsburgh, PA 15261

Prof. Alexander M. Cruickshank
Gordon Research Conference
Pastore Chemical Laboratory
University of Rhode Island
Kingston, RI 02881

DATE
ILME